



Solar Radiation and Climate Experiment (SORCE) X-Ray Photometer System (XPS): Final Data-Processing Algorithms

Thomas N. Woods¹ · Joshua Elliott¹

Received: 20 December 2021 / Accepted: 9 May 2022 / Published online: 30 May 2022
© The Author(s) 2022

Abstract

The *X-ray Photometer System (XPS)* is one of four instruments onboard NASA's *Solar Radiation and Climate Experiment (SORCE)* mission. The SORCE spacecraft operated from 2003 to 2020 to provide key climate-monitoring measurements of total solar irradiance (TSI) and solar spectral irradiance (SSI). The XPS is a set of photometers to measure the solar X-ray ultraviolet (XUV) irradiance shortward of 34 nm and the bright hydrogen emission at 121.6 nm. Each photometer has a spectral bandpass of about 7 nm, and the XPS measurements have an accuracy of about 20%. The updates for the final data-processing algorithms for the XPS solar-irradiance data products are described. These processing updates include improvements for the instrumental corrections for background signal, visible-light signal, and degradation trending. Validation of these updates is primarily with measurements from a very similar XPS instrument onboard NASA's *Thermosphere-Ionosphere-Mesosphere-Energetics-Dynamics (TIMED)* mission. In addition, the XPS Level 4 spectral model has been improved with new reference spectra derived with recent XUV observations from NASA's *Solar Dynamics Observatory (SDO)* and *Miniature X-ray Solar Spectrometer (MinXSS)* cubesat.

Keywords Solar irradiance · Solar-cycle observations · Instrument effects

1. Introduction

Solar ultraviolet (UV) radiation at wavelengths shorter than 320 nm is an important source of energy for terrestrial atmospheric processes. Solar UV photons are absorbed in Earth's atmosphere via photodissociation of molecules, photoionization of molecules and atoms, and photoexcitation including resonance scattering. The solar visible and infrared (IR) radiation at wavelengths longer than 320 nm is partially absorbed in the atmosphere, scatters off clouds and aerosols, and can reach the ground. The solar heating in the atmosphere and at

This article belongs to the Topical Collection:
The Solar Radiation and Climate Experiment (SORCE) Mission: Final Calibrations and Data Products
Guest Editor: Thomas N. Woods

✉ T.N. Woods
tom.woods@lasp.colorado.edu

¹ Laboratory for Atmospheric and Space Physics, University of Colorado, 3665 Discovery Dr., Boulder, CO 80303, USA

the surface is the primary energy input to the global climate system. Hence, accurate measurements of the solar total irradiance (TSI) and spectral solar irradiance (SSI) are critical for studying the radiative-energy balance, atmosphere photochemistry (such as the effects on ozone), and solar influence on global and regional climate change (e.g. Lean et al., 2005; Pilewskie, Rottman, and Richard, 2005; Ermolli et al., 2013). NASA's *Solar Radiation and Climate Experiment* (SORCE) observed both the TSI and SSI over its 17-year mission from 2003 to 2020. The focus here is on the SORCE *X-ray Photometer System* (XPS: Woods and Rottman, 2005; Woods, Rottman, and Vest, 2005) data in the X-ray ultraviolet (XUV) range of 0.1 nm to 34 nm and on the bright hydrogen emission at 121.6 nm. The XPS is the shortest-wavelength SSI instrument for SORCE. Solar XUV radiation photoionizes the neutral constituents of the terrestrial atmosphere and participates in the formation of the ionosphere. The photoelectrons created in this process interact further with the neutrals, leading to excitation, dissociation, and additional ionization. In addition, the excess energy from the absorption processes is a primary energy source for heating the thermosphere. The solar Lyman- α emission at 121.6 nm also contributes to the ionization in the lower D-region of the ionosphere and is a key energy input for the photochemistry of NO, H₂O, and O₃ in the mesosphere (Raulin et al., 2013).

The XPS instrument is designed to measure the solar XUV and Lyman- α irradiance in nine different broad bands with each photometer having a spectral bandpass of about 7 nm. The SORCE/XPS is almost identical to the XPS that is part of the *Solar Extreme-ultraviolet Experiment* (SEE) onboard NASA's *Thermosphere-Ionosphere-Mesosphere-Energetics-Dynamics* (TIMED) mission (Woods et al., 2005). The TIMED/SEE observations span 2002 to the present and thus fully overlap with the SORCE mission. The SORCE/XPS measurement at 121.6 nm overlaps with the far ultraviolet (FUV: 115–200 nm) measurements by SORCE's *SOLar STellar Irradiance Comparison Experiment* (SOLSTICE: McClintock, Rottman, and Woods, 2005; McClintock, Snow, and Woods, 2005; Snow et al., 2022). TIMED/XPS and SORCE/SOLSTICE provide important validation for SORCE/XPS data products.

There are also other measurements of the solar XUV irradiance that overlap with the SORCE mission. For higher spectral resolution measurements in the XUV range, there are the *EUV Variability Experiment* (EVE: Woods et al., 2012; Hock et al., 2012) measurements from NASA's *Solar Dynamics Observatory* (SDO). These EVE spectral irradiance measurements are at 0.1-nm spectral resolution with its *Multiple EUV Grating Spectrographs* (MEGS) with MEGS-A for the range of 6 nm to 37 nm and with MEGS-B for the range of 37 nm to 106 nm. EVE also has broadband measurements with about 2-nm bandpass with the *EUV SpectraPhotometer* (ESP: Didkovsky et al., 2012). As discussed in Section 4, the SDO/EVE spectra are used to improve upon the SORCE/XPS Level 4 data product that is a solar spectral model from 0.1 nm to 40 nm at 0.1-nm resolution. Another spectral measurement used in the SORCE/XPS Level 4 algorithm is solar X-ray spectra from the *Miniature X-ray Solar Spectrometer* (MinXSS) CubeSats (Mason et al., 2016; Woods et al., 2017; Moore et al., 2018). The third-generation spectrometer for the MinXSS project is called the *Dual-zone Aperture X-ray Solar Spectrometer* (DAXSS: Schwab et al., 2020), and the DAXSS measurement on the SDO/EVE calibration rocket flight in June 2018 is also used as a reference solar X-ray spectrum for the SORCE/XPS Level 4 algorithm. The *GOES X-Ray Sensor* (XRS) has a long record of the solar X-ray irradiance in two bands: 0.05–0.4 nm and 0.1–0.8 nm (e.g. Garcia, 2000). These GOES/XRS observations are also used in the SORCE/XPS Level 4 algorithm. Other solar XUV irradiance measurements overlapping with SORCE/XPS include those from the *Solar EUV Monitor* (SEM) onboard the *Solar and Heliospheric Observatory* (SOHO) (Judge et al., 1998), the *Solar Auto-calibrating*

Table 1 SORCE/XPS photometer parameters.

XPS diode number	Filter coating	Bandpass [nm]	Design thickness [nm]	Modeled thickness [nm]	Mission cadence (D, W, E)
1	Ti / C	0.1–7	500 / 50	387.5 / 50	D
2	Ti / C	0.1–7	500 / 50	387.5 / 50	W
3	Al / Sc / C	17–23	270 / 50 / 50	179.1 / 50 / 25	E
4	None (pinhole)	160–1000	—	—	E
5	Al / Nb / C	17–21	250 / 50 / 50	208.9 / 39.2 / 47.3	E
6	Ti / Mo / Au	0.1–11	40 / 200 / 100	45.2 / 111.3 / 74.1	E
7	Ti / Mo / Si / C	0.1–18	40 / 200 / 100 / 50	34.1 / 131.3 / 103.5 / 46.1	D
8	None (pinhole)	160–1000	—	—	W
9	Al / Cr	0–7, 27–37	270 / 100	175 / 114.4	E
10	Al / Mn	0–7, 25–34	270 / 100	175 / 144.7	D
11	Acton Ly- α ($\times 2$)	121–122	—	—	W
12	None (pinhole)	160–1000	—	—	E

The modeled thicknesses for the XUV filter coatings were determined using pre-flight calibrations at NIST SURF. The Mission cadence categories are related to the observation cadence after the XPS filter-wheel anomaly in December 2005. Those categories are: **D** = Daily observations, **W** = Weekly observations, and **E** = End-of-mission calibration observations.

EUV Spectrometers (Sol-ACES) onboard the *International Space Station* (ISS) (Schmidtke et al., 2006), the *Large Yield Radiometer* (LYRA) onboard PROBA2 (Hochedez et al., 2006), the *Solar Photometer in X-rays* (SphinX) onboard CORONAS/PHOTON (Sylwester et al., 2012), and the *Solar X-ray Monitor* (SXM) onboard *Chandrayaan-2* (Mithun et al., 2020).

2. XPS Instrument Overview

Woods, Rottman, and Vest (2005) provide details of XPS optical, mechanical, electrical, and software designs and operational modes. They also describe the XPS science-processing algorithms and the pre-flight calibrations at the National Institute of Standards and Technology (NIST) Synchrotron Ultraviolet Radiation Facility (SURF) (Arp et al., 2000). Briefly, XPS has 12 photometers with eight being for the XUV range, one for the bright H I Lyman- α emission at 121.6 nm, and three for measuring the visible-light transmission of its calibration windows. The XUV filters on eight of the photodiodes are thin-film filters deposited directly onto the photodiode to avoid using delicate free-standing metal-foil filters that are difficult to handle, prone to develop pinholes, and degrade with time. Narrow-band interference filters are used for the Lyman- α measurement, and there are no filters for the three visible-light photodiodes. XPS measures the very energetic XUV irradiance that has solar-cycle 11-year variability that exceeds a factor of 100 at the shortest wavelengths and a factor of three for the He II 30.4 nm emission. In order to precisely measure this amount of solar variability, the XPS has measurement requirements of 10% precision and 20% relative accuracy. Table 1 lists the XPS photometers, their filter bandpasses, and observation cadence during the SORCE mission. Woods and Rottman (2005) is a companion article for XPS to describe early mission science results from SORCE/XPS. Another key reference for XPS

data processing is Woods et al. (2008), which describes the original XPS Level 4 spectral model for the solar XUV irradiance using the SORCE/XPS photometer data.

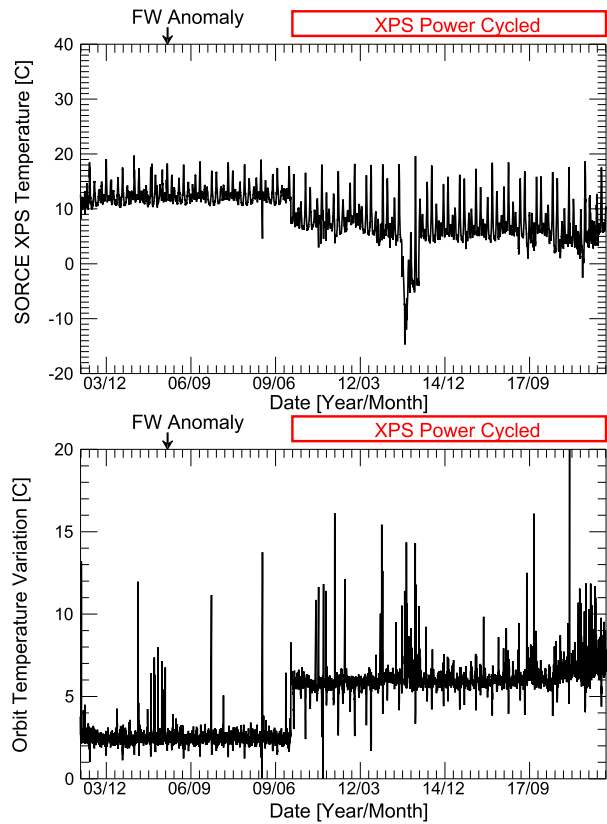
The XPS has a filter-wheel mechanism with eight discrete positions so that the dark (thermal) signal, visible-light signal, and solar XUV signal can be accurately measured from each photometer. As there are only three solar-irradiance measurements made at any one filter-wheel position, a complete solar observation for the twelve XPS photodiodes involves four different filter-wheel positions. The other four filter-wheel positions are for dark measurements. Woods, Rottman, and Vest (2005) provide a more detailed overview of the XPS filter-wheel mechanism and the XPS measurement configuration at each filter-wheel position (e.g. see Table 1 and Figure 3). XPS has had one flight anomaly whereby the filter-wheel mechanism was temporarily frozen in one position in December 2005. The mechanism freed itself with another command to move the mechanism. As a conservative approach, the movement of the XPS filter-wheel mechanism was minimized for the remaining part of the SORCE mission. This anomaly did not reappear since it happened in December 2005.

Prior to the XPS filter-wheel anomaly, the XPS observations included stepping the filter-wheel mechanism through a sequence of filter positions so that dark (blocked aperture), visible-light (fused-silica window), and solar (clear aperture) measurements are made for each photodiode over a period of about five minutes. The cadence for the XPS photodiode integrations was ten seconds then. These observations were made continuously during the solar side of the SORCE orbit. Once a week, a special calibration experiment was executed to focus on observations of the four visible-light photodiodes for tracking the degradation of the six fused-silica windows in the XPS filter wheel and for longer solar observations of the three redundant XPS photometers. Woods, Rottman, and Vest (2005) describe these normal observations for XPS.

After the XPS filter-wheel anomaly, the XPS observations were limited to using the filter-wheel position #6 for most of the time. This filter-wheel position provides the most critical solar observations using one of the 0.1–7 nm irradiance channels and two other XUV channels to cover up to 34 nm. On a regular cadence (once a week), the filter wheel would be moved to three other positions for limited fused-silica-window measurements and redundant channel measurements for tracking degradation of the primary channels. XPS measurements made during orbit-eclipse periods provide dark measurements without having to move the filter wheel.

As discussed by Woods et al. (2021), the most significant SORCE spacecraft anomaly was the degradation of its battery capacity, which required managing spacecraft and instrument power so that lower priority subsystems were turned off during orbit eclipse. The most challenging battery-capacity degradation happened in July 2013, when the SORCE largest data gap began. With modifications to the SORCE operations, normal solar observations were restarted in March 2014 and continued successfully up to the spacecraft passivation in February 2020. Woods et al. (2021) also provide a summary of other shorter data gaps during the SORCE mission. Being a lower priority instrument for SORCE, the XPS was turned off during orbit eclipse as a power-saving option starting in 2010. At that time, the XPS integration period changed from 10 seconds to 65 seconds to reduce its daily data volume, and the weekly calibrations changed to a monthly cadence. The power cycling of XPS changed the temperature trending for XPS, as shown in Figure 1. Notably, the XPS temperature is cooler by a few degrees starting in 2010, and there is more orbital variation of its temperature once power cycling started for XPS.

Figure 1 Mission trend of XPS daily average temperature (*top*) and orbital variation of its temperature (*bottom*). Orbital variation is the maximum minus minimum temperature in an orbit. The orbital variation of the XPS temperature increased from about 3 °C to about 6 °C after XPS started being power cycled in 2010.



3. Revisions for XPS Science Data-Processing Algorithms

Woods, Rottman, and Vest (2005) describe the XPS science data-processing algorithms. While those algorithms are still used for the final Version 12 data products, there are several improvements for instrumental trending as derived from in-flight calibrations. Those improvements include better trending of the dark signal as a function of time and temperature, better trending of the visible-light signal as a function of time, long-term trending of the degradation for the visible-light (fused silica) windows, and long-term trending of the degradation for the XUV and Lyman- α filters. Each of those corrections is described after presenting a summary of the irradiance conversion for the XPS measurements. A simplified version of the irradiance algorithm is shown in Equation 1; the details of this algorithm are described by Woods, Rottman, and Vest (2005).

$$E_i = \frac{(I_{i,\text{total}} - I_{i,\text{dark}} - I_{i,\text{visible}}) f_{i,\text{Degrade}}}{R_i f_{i,\text{xuv_fov}}} \quad (1)$$

The irradiance [E_i] is for photodiode number i in units of W m^{-2} and is the key result in the XPS Level 2 data products. The daily average of the XPS Level 2 irradiances is provided in the XPS Level 3 data products. The responsivity [R_i] is a static value in units of $\text{nA}(\text{W m}^{-2})^{-1}$ that was derived with pre-flight calibrations and is presented in more detail by Woods, Rottman, and Vest (2005). The three signal terms $I_{i,\text{total}}$, $I_{i,\text{dark}}$, and $I_{i,\text{visible}}$ are

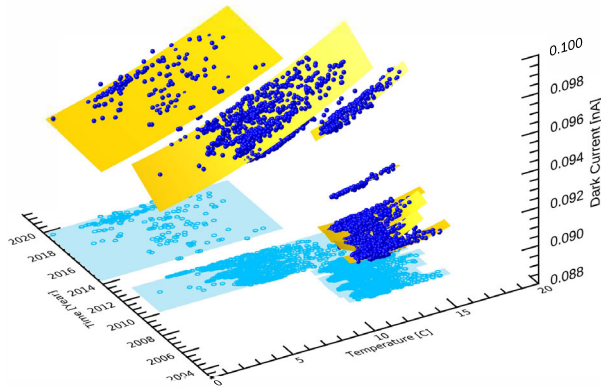


Figure 2 Example of dark-signal trending for XPS photodiode #1. The dark model has piecewise fits with linear trending in time and a quadratic fit in temperature for each time period between the discrete shifts of the electrometer's offset. The *dark-blue dots* are the measured dark signals, and the *yellow surfaces* are the dark-signal model used in XPS data-processing algorithm. The dark-signal data and model fits are projected down to the Time–Temperature plane as *light blue* to illustrate better the temperature-range changes over the mission.

the photodiode currents in units of nA for the total signal, dark signal, and visible signal, respectively. The total signal is measured with a cadence ranging from 10 seconds to 65 seconds. The dark signal was originally measured about every five minutes early in the mission, but it is now a model of the dark signal as a function of time and temperature based on the photodiode dark measurements over the full mission. The visible signal represents the visible-light (out-of-band) contamination, and it includes correction for the transmission of the visible-light window (fused silica) and field-of-view (FOV) corrections for those visible-signal measurements. Like the dark measurements, the visible signal was originally measured about every five minutes early in the mission, but it is now a model of the visible signal as a function of time. The SORCE spacecraft pointing towards the Sun is very stable (a few arc-minutes) for the solar observations over the full mission; nonetheless, a FOV correction [$f_{i,\text{xuv_fov}}$] is applied. These FOV corrections are unitless as they are normalized to the response at the FOV-map center point. The instrumental-degradation trend as a function of time is the $f_{i,\text{Degrad}}$ term. The degradation correction is unitless as it is normalized to the response at the beginning of the mission. The models for dark signal and visible signal for each photodiode [i] as used in XPS Version 12 data products are discussed next.

The dark signal is a combination of an intentional offset applied to the sensor electrometer and the thermal-background signal from the photodiode. The electrometer for each photodiode consists of a current operational amplifier (Analog Devices AD549RP) and a voltage-to-frequency converter (Analog Devices AD650). From pre-flight radiation testing, both of the electrometer parts were known to be able to have small and permanent shifts in their offset level from energetic particles impinging on them. These offset shifts can be positive or negative, and these shifts have happened randomly a few times over the 17-year mission. The same type of electrometer is also used in the TIMED/SEE-XPS and SDO/ESP photometers, and those also experience these small, discrete shifts in their dark signals during their missions. An example of the dark-signal data and model is shown in Figure 2 for XPS photodiode #1. Because of these discrete shifts over the mission, the dark-signal model has piecewise fits with linear trending in time and quadratic fit in temperature for each time

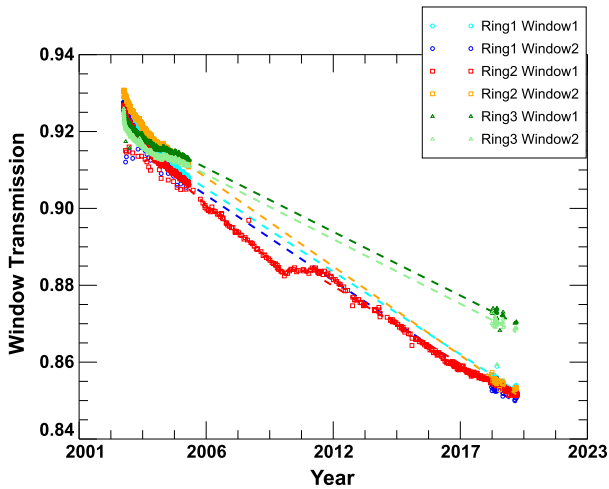
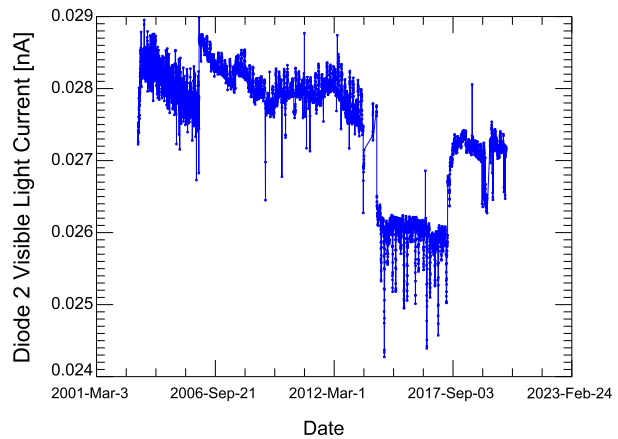


Figure 3 Transmission trends of the fused-silica windows. There are a total of six windows in XPS to track the XUV photodiode visible-light signal. The windows are organized with a redundant pair of windows in each of the three rings in the XPS filter wheel. The transmission measurements for all windows were made frequently before the filter-wheel anomaly in December 2005 and also made during the last few months of the mission. The Ring-2 Window-1 transmission was measured about once a week over the entire mission period. The *dashed lines* are the estimated trend for transmission degradation over the mission.

period between the electrometer shifts. That is, there is a different dark-signal model fit for each time period between discrete shifts in the dark signal. The dark-signal model is used in data processing from 2006 to 2020 using daily/weekly dark-signal measurements. Prior to 2006, there are dark-signal measurements every five minutes, and those are used directly instead of a dark-signal model. The in-flight measurements of the dark signal as a function of temperature are consistent with pre-flight calibrations that revealed that most of this temperature dependence is in the electrometer parts and not as much related to the Si photodiodes' thermal effects. The XPS photodiodes are International Radiation Detectors AXUV-100 Si photodiodes, and they have very small thermal background signals because of their high shunt resistance.

The visible signal represents the photodiode signal that is out of band from the XUV bandpass. This visible signal is measured using fused-silica windows in the XPS filter wheel. The visible-signal contribution for the XUV photodiodes did not change much over the mission, but the transmission of the fused-silica windows did degrade steadily over the mission by about 1% per year. The window-transmission degradation is measured in-flight by having bare (visible-light sensitive) photodiodes in XPS. There are six fused-silica windows in the XPS filter wheel, and the transmission trends of those windows are shown in Figure 3. Four windows degraded at about the same rate, and there are two windows that degraded at a slightly slower rate. There is an odd break in the window-degradation trending in 2010–2012 that may be related to the time when XPS power cycling began and reduced the operating temperature for XPS (see Figure 1). However, we do not have a plausible explanation for why the window degradation resumed its trend in 2012. As explained by Woods, Rottman, and Vest (2005), the visible signal used in the irradiance Equation 1 is the measured signal of the XUV photodiode when the window is in place divided by the transmission of the window. An example of the visible-signal trend over the mission for XPS photodiode #2 is shown in Figure 4. The slow downward trend may be related to diode

Figure 4 Example of visible-light signal trend for XPS photodiode #2. The slow downward trend may be related to photodiode degradation in visible wavelengths. The discrete jumps in the visible signal could be related to pinholes developing in the XUV foil filter for photodiode #2 and/or spacecraft operational changes that caused temperature drifts that are not fully corrected in the dark-signal model.



degradation at visible wavelengths. The discrete jumps in the visible signal could be related to pinholes developing in the XUV foil filter for photodiode #2 and/or spacecraft operational changes that caused temperature drifts that are not fully corrected in the dark-signal model. It is not clear what causes the short-duration upward spikes in the visible-signal trends. These variations of the visible-light signal are smaller than the dark signal for photodiode #2, so imperfections for its dark model can impact the trend of the visible-light signal.

The dark-signal and visible-signal trends are relatively minor corrections as compared to the $\times 100$ variability for the solar XUV observations. The photodiode and XUV filter-degradation trends over the *SORCE* mission are also small for most of the XUV photodiodes, but the degradation trend of the Lyman- α interference filter is larger. The onboard tracking of the instrument degradation includes three redundant XUV photometers and comparisons to the *SORCE/SOLSTICE* measurements for the XPS Lyman- α photometer. There have also been regular (about annual) underflight calibration flights for *TIMED/SEE* and *SDO/EVE* to provide additional verification for the degradation trends for the *SORCE/XPS* channels.

We anticipated that the XUV photometers should have only minor degradation during flight due to using radiation-hardened photodiodes and the pre-flight technology development at International Radiation Detectors (IRD) of having the XUV filters directly deposited onto the photodiodes. As noted earlier, the XUV filters are thin-film filters deposited directly onto the photodiode to avoid using delicate free-standing metal-foil filters. In addition, the IRD AXUV-100 photodiodes are specifically designed to be robust and very radiation-hardened (1 Grad) photodiodes for spaceflight applications. While most of the XUV photometers on *TIMED* and *SORCE* are very stable (e.g. see Figure 5 for *SORCE/XPS* photodiode #1 degradation trend), the *SORCE/XPS* photodiode #7 indicates more significant degradation of about 5% year $^{-1}$ (see Figure 6). The steady decline of sensitivity over the *SORCE* mission is suggestive of oxidation of the XUV filter, instead of degradation by hydrocarbon contamination, which normally shows exponential decay over a mission (a lesson learned with *SDO/EVE* foil-filter analysis: BenMoussa et al., 2013). Both of these degradation trends shown in Figures 5 and 6 are based on comparing to the *TIMED/SEE* 0.1–7 nm photometer, which has not indicated any measurable degradation trending over the *TIMED* mission. The *TIMED/SEE* solar observations are limited to 3% duty cycle, as compared to *SORCE* solar observations with $\approx 65\%$ duty cycle, and so *TIMED/SEE-XPS* channels are expected to degrade much more slowly than *SORCE* channels. Furthermore,

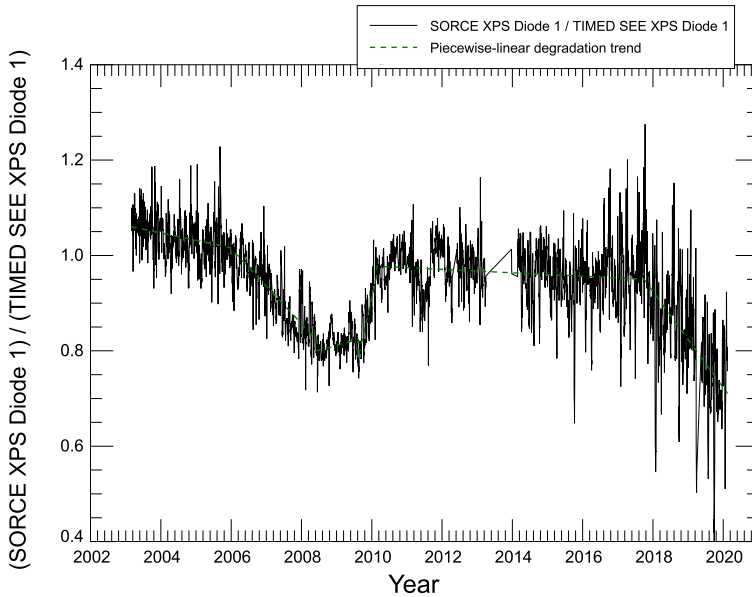


Figure 5 Degradation trend for SORCE/XPS photodiode #1. This degradation trend is derived by comparing to the TIMED/SEE-XPS 0.1–7 nm photometer, which has not indicated any measurable degradation trending over the TIMED mission. The dips in this ratio during solar-cycle minima in 2008–2009 and 2019–2020 probably reflect differences more in the dark-signal correction than in instrument degradation.

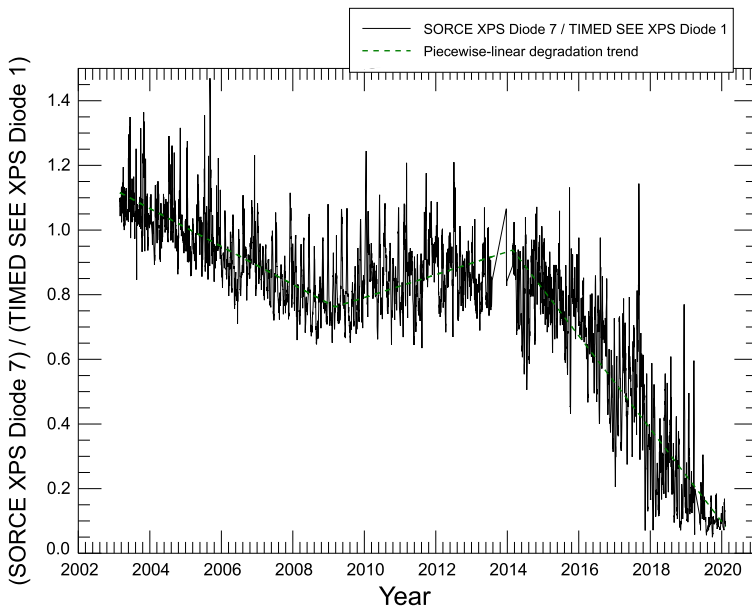


Figure 6 Degradation trend for SORCE/XPS photodiode #7. This degradation trend is derived by comparing to the TIMED/SEE-XPS 0.1–7 nm photometer. The SORCE/XPS photodiode #7 bandpass includes contributions from both 0.1–7 nm and 7–18 nm, so this comparison can also have solar-variability differences between those two band passes. The trend between the cycle minimum in 2008–2009 to the cycle minimum in 2019–2020 may better represent the true instrument-degradation trend for XPS photodiode #7.

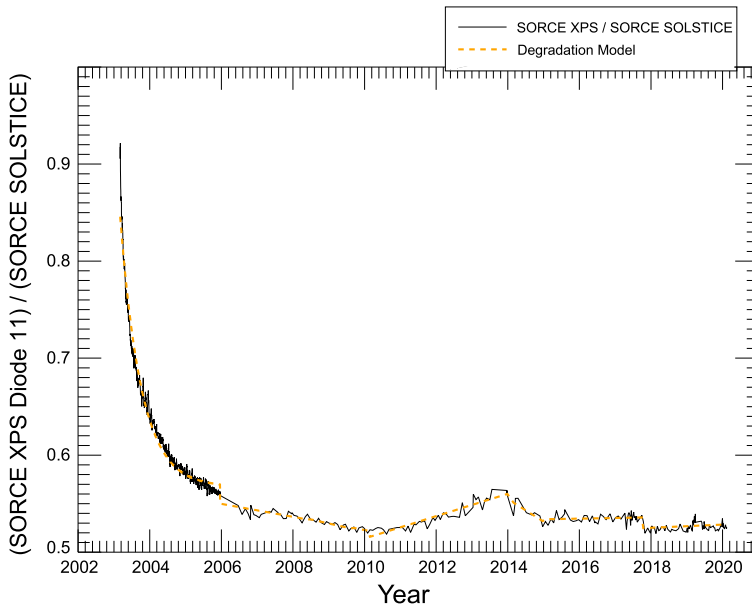


Figure 7 Degradation trend for SORCE/XPS Lyman- α photometer (photodiode #11). This degradation trend is derived by comparing to the SORCE/SOLSTICE Lyman- α observations that have been corrected with its own redundant-channel calibrations and with stellar calibrations.

the TIMED/SEE underflight calibration-rocket experiments have verified that the SEE-XPS channels have degraded no more than 1% over the 20-year TIMED mission. However, there is the possibility that the decrease of about 20% near 2009 in Figures 5 and 6 could be caused by the uncertainty for the visible-light signal correction for the TIMED/SEE-XPS photometer #1 because there have not been visible-light measurements for TIMED/SEE-XPS since its filter-wheel failure in 2002 and because visible-light contributions are maximized during low solar activity periods.

We did anticipate that the Lyman- α interference filters would degrade in space based on similar Acton UV interference filters on SOLSTICE onboard the *Upper Atmosphere Research Satellite* (UARS) having moderate degradation over time (Woods et al., 1998). The SORCE/SOLSTICE observations, which are corrected with its own redundant channel calibrations and with stellar calibrations, are used to estimate the degradation trend for the XPS Lyman- α photometer (photodiode #11). In order to compare SORCE/SOLSTICE Lyman- α measurements with 0.1-nm spectral resolution to the broadband XPS measurement, we weight the SOLSTICE high-resolution Level 3 spectrum by the XPS photodiode #11 responsivity function, and then integrate over wavelength. This convolved-integrated result can then be compared directly to the XPS Lyman- α photometer measurement. This comparison, as shown in Figure 7, shows a rapid degradation for the XPS Lyman- α filter during the first year of the SORCE mission, suggesting that hydrocarbon contamination could be the leading cause of this degradation.

The Acton interference filters used for XPS photodiode #11 are known to degrade in space from any hydrocarbon contaminants on the optic that can be polymerized with solar exposure and also from high-energy particle radiation affecting the multilayer filter transmission (Woods et al., 1998). The XUV filters are less sensitive to those optical-degradation

effects due to X-rays having very high transmission through most materials. However, hydrocarbons and oxidation absorption of solar XUV radiation begins to ramp up longer than about 15 nm; this may explain why XPS photodiode #7, with its bandpass extending out to 18 nm, has more degradation than XPS photodiode #1 with its bandpass limited to shorter than 7 nm.

Changes in solar exposure over the mission most likely play a role in these degradation trends. The number of solar observations does not change much over the mission, even with the change in operations in 2010 to power-cycle the XPS every orbit-eclipse period. However, the amount of solar X-ray radiation changes by more than a factor of ten over the solar cycle. Notably, there appears to be recovery for the photometer sensitivities during 2010–2014 following the solar minimum in 2008–2009 (see Figures 5–7). Perhaps the reduced amount of solar X-ray radiation exposure during the solar-cycle minimum may have enabled a time for some recovery for the windows and photodiodes before the solar activity picked up again in 2011. However, the XPS trends do not follow well a solar-cycle pattern, as one might expect for effects due only to solar exposure.

4. New Reference Spectra for XPS Level 4 Spectral Model

The XPS Level 4 data product is a model estimate of the solar irradiance at higher spectral resolution than the XPS broad-band measurements. The original version of this Level 4 product (Woods et al., 2008) used three variability components based on CHIANTI model spectra (Dere et al., 1997; Landi et al., 2013; Del Zanna et al., 2015). Those three components have two reference spectra for the quiet Sun [E_{QS}] and active region [E_{AR}] and a third flare-component spectrum [E_F]. The two reference (static) spectra are used to model the daily variations by adjusting the fraction of the solar disk covered by active regions to match the XPS 0.1–7 nm daily minimum irradiance. The flare component is for the XPS 0.1–7 nm irradiance above its daily minimum irradiance and is based on using an isothermal CHIANTI spectrum with the coronal temperature derived with GOES/*X-Ray Sensor* (XRS) data (Garcia, 2000). As indicated in Equation 2, the XPS Level 4 model irradiance is derived by using the magnitude of the XPS irradiance for its 0.1–7 nm channels to determine the active-region scaling [f_{AR}] for daily variability and to scale the flare spectrum [f_F] for the one-minute cadence of the Level 4 product output [E_{L4}]. These scale factors are derived with the integrated 0.1–0.7 nm model irradiance through comparison to the XPS broadband measurement, and then the Level 4 spectral irradiance is calculated for all wavelengths between 0.1 and 40 nm using the reference spectra with those scale factors. This Level 4 algorithm is described in more detail by Woods et al. (2008):

$$E_{L4} = E_{QS} + f_{AR}E_{AR} + f_F E_F(T). \quad (2)$$

The new update for the XPS Level 4 product is an improvement of the reference spectra for the quiet Sun (QS) and active region (AR) based on measurements from SDO/EVE, MinXSS, and SphinX. The flare component for the updated Level 4 product is the same as the original Level 4 product model. This update for the QS and AR reference spectra is one of the largest changes for the final XPS Version 12 data set. This update is also the most significant from a science viewpoint because the new Level 4 spectra have a more accurate spectral profile over the 0.1–40 nm range. This improvement is because these updated reference spectra are mostly based on measurements instead of the original CHIANTI model spectra. The following describes how the new reference spectra were derived.

The new QS and AR reference spectra are derived using the SDO/EVE measurements in the 6 nm to 40 nm range, new solar X-ray irradiance measurements at wavelengths shorter than 1 nm, and new spectral modeling for the 1–6 nm gap between those measurements. For deriving the new reference spectra for wavelengths in the 6–40 nm range, the XPS 0.1–7 nm daily irradiance is used as the variability proxy for the SDO/EVE Level 3 (daily average) measurements with its 0.1-nm spectral resolution from May 2010 to June 2014. The linear fits between the XPS variability proxy and the EVE spectra at each wavelength provide the new values for the reference spectra at each wavelength. In particular, the y -intercept of the fit is for the QS reference spectrum (solar-cycle minimum), and the slope (normalized by variability proxy maximum) is for the AR reference spectrum. This approach of using all of the EVE data, versus just picking two reference days during the SDO mission, provided more accurate results for the two reference spectra needed for the XPS Level 4 model. The X-ray data sets are not long enough to also do a proxy model derivation, so two reference spectra in the X-ray range are used instead. The SphinX 2009 solar-cycle minimum spectrum (Sylwester et al., 2012) is used for the QS reference spectrum, and the MinXSS calibration-rocket experiment measurement in June 2018 (Schwab et al., 2020) is used for the AR reference spectrum.

The spectral gap from 1 nm to 6 nm is filled using CHIANTI spectra calculated using differential emission measure (DEM) fits to the SDO/EVE spectra in the 10–14 and 26–30 nm ranges and X-ray reference spectra at wavelengths shorter than 1 nm. The DEM fitting is similar to the technique described by Warren, Mariska, and Doschek (2013). In particular, multiple DEM Gaussian profiles are used with logarithmic temperature (K , $\log(T)$) peaks every 0.2 and with Gaussian width of 0.42 in $\log(T)$ (FWHM of 1.0). The reference spectra and DEM fits are shown in Figure 8. This QS DEM is very similar to the QS DEM derived with *EUV Imaging Spectrograph* (EIS) observations (diamonds in Figure 8). These QS and AR DEMs both have smaller emission measure (EM) at $\log(T)$ greater than 6.2 than the standard QS and AR DEMs in CHIANTI. In summary, the adopted reference QS and AR spectra for the Level 4 processing consists of the measurements and the DEM spectra in the 1–6 nm range to fill the gap between the measurements. As mentioned earlier, these reference (static) spectra are used for the daily minimum irradiance, and the flare-component spectra is more dynamic with the isothermal corona temperature calculated every minute with GOES/XRS data and scaled to describe the irradiance above the daily-minimum irradiance. The new reference QS and AR spectra are the only changes from the Woods et al. (2008) algorithm used for the XPS Level 4 model.

The solar-cycle variability for XPS Level 4 is presented to show the comparison of the new reference spectra used in XPS Version 12 to the original XPS Level 4 reference spectra in XPS Version 10. Woods et al. (2022) present some solar-cycle variability results during the SORCE mission, and their dates for Solar Cycle 24 minimum and maximum are chosen for this comparison. Namely, the maximum is selected to be the 217-day average centered on 2011/351 (the 351st day of 2011), and the 2008–2009 minimum is the 217-day average centered on 2008/315. These cycle-minimum and -maximum spectra are compared between the XPS Version 12 and XPS Version 10 in the Figure 9 top-left panel. This comparison highlights that there are significant differences between these two versions of the XPS Level 4 product and that those differences are mostly independent of solar activity. The Solar Cycle 24 variability (maximum minus minimum) is shown in Figure 9 bottom-left panel. The largest amount of solar-cycle variability (in energy units) from a single emission line is from the He II 30.4 nm emission (0.10 mW m^{-2} , or 8.5% of 0.1–40 nm total variability). The many iron lines in the XUV range are also major contributions to the variability. For example, the iron lines identified in Figure 9 contribute 30% of the total variability in the

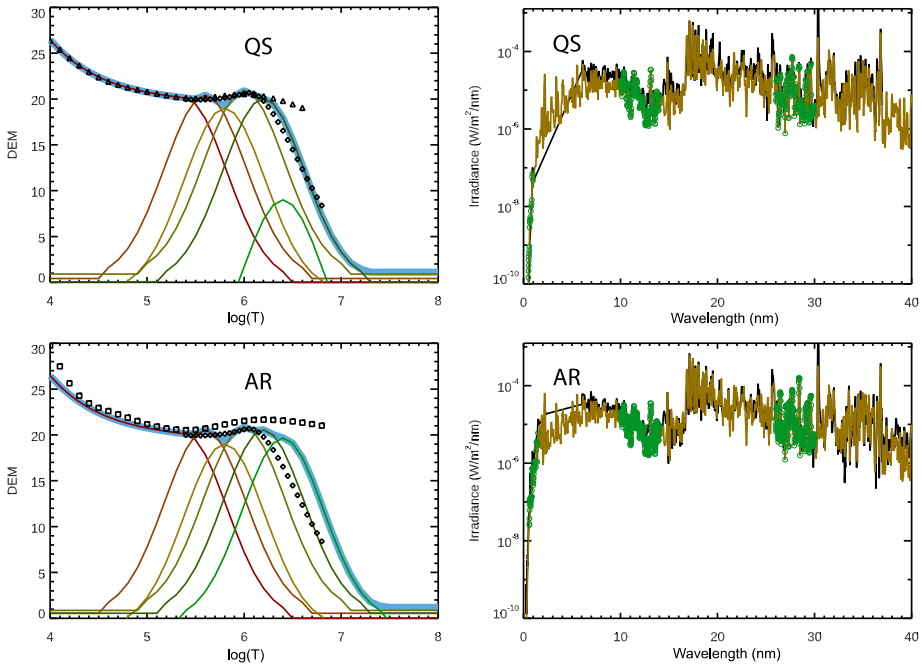


Figure 8 DEM results for XPS Level 4 spectral model. The quiet-Sun (QS) DEM (*top left*) is derived from SDO/EVE and SphinX measurements (*top right*). The active-region (AR) DEM (*bottom left*) is derived from SDO/EVE and DAXSS measurements (*bottom right*). The derived DEMs in the *left plots* are the *thick light-blue lines* that are the combination of multiple DEM Gaussian profiles in color. Some standard CHIANTI DEM profiles are also shown: *triangles* are the CHIANTI QS DEM, *diamonds* are the EIS QS DEM, and *squares* are CHIANTI AR DEM. In the *right plots*, the *black lines* are the measurements, the *gold lines* are the DEM-based spectra, and *green symbols* are for the parts of the measurement used for deriving the DEM. The adopted reference spectrum includes the measurements and the DEM spectra in the 1–6 nm range to fill the gap between the measurements.

0.1–40 nm range. Also interestingly, each iron emission from Fe IX to Fe XVI has a similar amount of solar-cycle variability of about 0.02 mW m^{-2} (or 2% of the 0.1–40 nm total). We note that the line irradiance is in units of mW m^{-2} from integrating over wavelength of the spectral irradiance in units of $\text{mW m}^{-2} \text{ nm}^{-1}$. From a relative change [%] viewpoint, the solar-cycle variability relative to the minimum irradiance is about 100% (factor of 2) for most wavelengths, and then there is a sharp rise in relative variability to factors of 10 to 1000 at wavelengths shorter than 2 nm.

Woods et al. (2022) provide more discussion about these solar-cycle variability results from SORCE, as well as showing favorable comparison to SSI composites developed with SORCE data. It is also useful to compare these new XPS Level 4 model spectra to the predictions from the Flare Irradiance Spectral Model (FISM Version 2; Chamberlin et al., 2020). This comparison is shown in the Figure 9 right panels. The FISM2 development used the SORCE/XPS Level 4 Version 11 product for wavelengths shorter than 6 nm, SDO/EVE MEGS-A Level 2 Version 6 spectra for wavelengths between 6 nm and 37 nm, and SDO/EVE MEGS-B Level 2 Version 6 spectra for wavelengths longer than 37 nm. The SORCE/XPS Level 4 Version 12 product and FISM2 predictions agree very well (within 20%) for most wavelengths because they use very similar SDO/EVE data sets for development. The largest differences are for wavelengths longer than 37 nm because FISM2 used

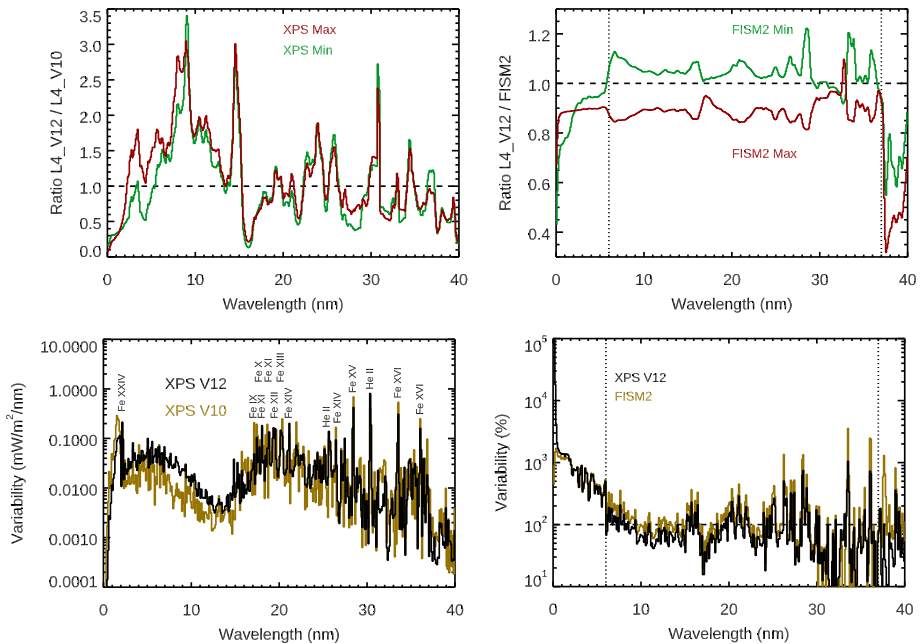
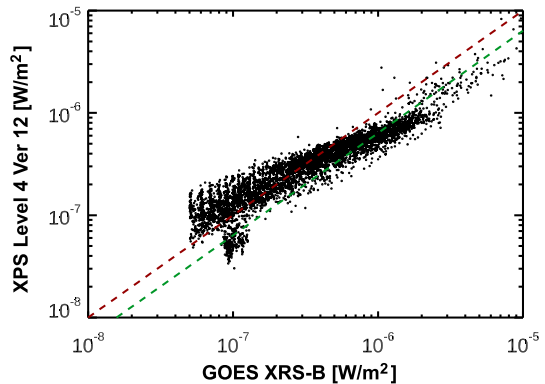


Figure 9 XPS Level 4 spectra and FISM2 model spectra are compared for solar-cycle variability study with the Solar Cycle 24 maximum being 217-day average centered on 2011/351 and with 2008–2009 minimum being a 217-day average centered on 2008/315. (*top left*) Comparison of XPS Level 4 solar-cycle maximum and minimum spectra for Version 12 (final product with new QS and AR reference spectra) and Version 10 (use of CHIANTI QS and AR reference spectra). There are systematic differences for most wavelengths independent of solar activity. (*top right*) Comparison of XPS Level 4 Version 12 to FISM2 for the maximum and minimum spectra. There is good consistency between them for wavelengths lower than 37 nm. (*bottom left*) The solar-cycle variability, calculated as maximum minus minimum, are similar for XPS Level Versions 12 and 10 down to about 12 nm, and Version 12 shows more variability for 3–12 nm and less variability for 0–2 nm than for Version 10. (*bottom right*) The solar-cycle relative variability values [%] are compared for XPS Level 4 Version 12 to FISM2 predictions. The FISM2 variability results are about 25% higher than XPS Level 4 results.

MEGS-B Version 6 data versus SORCE/XPS Level 4 Version 12 that used MEGS-B Version 7 data. Because of the systematic differences for the reference spectra for cycle minimum and maximum as shown in Figure 9 top-right, the FISM2 solar-cycle variability is about 25% more than the XPS Level 4 Version 12 variability, as shown in Figure 9 bottom-right panel. This difference is reasonable considering that the uncertainties for the XPS Level 4 product are about 30%.

The changes in the reference spectra between Versions 12 and 10 are most notable at wavelengths shorter than 17 nm and for the He II 30.4 nm emission, as shown in Figure 9 top-left panel. The difference for the optically thick He II 30.4 emission was expected in that the CHIANTI model is more appropriate for optically thin emissions. The differences at wavelengths shorter than 17 nm may be partially related to several atomic emission lines being missing in the earlier CHIANTI version used for the XPS Version 10 (Woods et al., 2008). The uncertainties for the XPS Level 4 Version 10 irradiances are 30–50%. The uncertainties for the Level 4 Version 12 irradiances are improved to about 20% for the 0.1–1 nm and 6–40 nm ranges where there are spectral irradiance measurements, but the uncertainties for the 1–6 nm range remain at 30–50%. Hence, the uncertainties for the ratio

Figure 10 Comparison of GOES/XRS-B 0.1–0.8 nm irradiance to XPS Level 4 Version 12 integrated over 0.1–0.8 nm range. The *green-dashed* line is the linear fit of GOES XRS-B and XPS irradiance. The *red-dashed* line is the 1-to-1 line.



of Version 12 to Version 10 irradiances are 40–70% for the 1–6 nm range and 35–55% for the other wavelengths. While there are systematic differences for most wavelengths independent of solar activity, there are solar-cycle-related differences for the wavelengths shorter than 12 nm. Those differences are also clear in the solar-cycle variability shown in the Figure 9 bottom-left panel. That is, the XPS Version 12 indicates more solar-cycle variability than XPS Version 10 for the 2–12 nm range, but the XPS Version 12 variability is less than XPS Version 10 results for the 0.1–2 nm range. The shortest-band differences can be validated with comparisons to GOES XRS measurements, as discussed next.

Prior to this update for the XPS Level 4 reference spectra, the XPS Level 4 Version 10 irradiance integrated over the 0.1–0.8 nm range was 4.4 times larger than the GOES/XRS-B irradiance level. This comparison has the standard GOES/XRS-B calibration already applied to XRS-B (factor of 1.42 increase: www.ngdc.noaa.gov/stp/satellite/goes/doc/GOES_XRS_readme.pdf). Now, the XPS Level 4 Version 12 product and GOES/XRS irradiances for the 0.1–0.8 nm band are in much better agreement, as illustrated in Figure 10. The linear fit between GOES/XRS-B and XPS Level 4 (green-dashed line in Figure 10) indicates that XPS is 37% lower than XRS-B. However, the relationship between them is more complicated than a single linear term, as discussed further by Hock, Woodraska, and Woods (2013) from comparing GOES/XRS to another similar broadband X-ray photometer onboard SDO/EVE. This GOES/XPS comparison provides partial validation for the new XPS Level 4 reference spectra.

This same Level 4 algorithm and reference spectra are also used for the TIMED/SEE-XPS and SDO/EVE-ESP data processing. The TIMED/SEE-XPS has two identical Ti/C-coated photodiodes to that on SORCE/XPS, and those are also used as the proxy for the SEE-XPS Level 4 algorithm. The EVE-ESP zeroth-order channel has a similar bandpass of 0.1–7 nm, but it consists of an Al/C foil filter and a Ti/C foil filter along with a transmission grating and a quadrant photodiode. As the ESP bandpass is similar, the XPS Level 4 algorithm is a good fit for using the ESP 0.1–7 nm photometer data as the variability proxy. The ESP Level 4 algorithm has an additional change of using a reference-flare spectrum based on SDO/EVE flare spectra, instead of using isothermal CHIANTI spectra and the GOES/XRS data for the flare temperature. This simplification for ESP Level 4 assumes a coronal flare temperature of about 10 MK and has the advantage of not requiring GOES/XRS data for the EVE-ESP Level 4 processing.

5. Summary

The SORCE/XPS has provided solar spectral irradiance results from 2003 to 2020 for the XUV 0.1–40 nm range and for the bright hydrogen emission at 121.6 nm. The XPS final data product is its Version 12 product, and this product includes recent improvements for the instrumental corrections for background signal, visible-light signal, and degradation trending. In addition, the XPS Level 4 spectral model has been improved with new reference spectra derived with solar EUV observations from SDO/EVE and with recent solar SXR observations. Examples of solar-cycle variability for the SORCE/XPS data are shown here, as well as by Woods et al. (2022). The He II 30.4 nm emission and many Fe lines are key contributors to the solar-cycle variability for the XUV range of 0.1–40 nm.

Similar broadband measurements of the solar XUV irradiance are being continued by the TIMED/SEE-XPS and the SDO/EVE-ESP. Of course, the longest-running record is for the GOES/XRS X-ray bands below 1 nm, which started back in the 1970s and is expected to continue for many more decades by the NOAA Space Weather operational program. The more recent GOES series also has the *EUV Sensors* (EUVS) for a few bands in the EUV down to 17 nm, but there are no GOES solar-irradiance observations between 1 nm and 17 nm. As both TIMED and SDO are older spacecraft that have had multiple mission extensions, there is a serious risk of having spectral gaps in monitoring the solar XUV and EUV ranges. It is conceivable that the next-generation GOES-VW solar EUV and X-ray instruments might be able to fill any such spectral gaps, but probably not until the 2030s. The MinXSS cubesat (Mason et al., 2016, 2020) and CSIM cubesat (Richard et al., 2019) have demonstrated that small satellites can make solar-irradiance observations, so new solar-irradiance measurements from small research satellites could reduce the risks of measurement gaps, both in time and in wavelength. One such example is the CubIXSS cubesat recently selected for studying flares in the SXR range, and it also has the capability for solar-irradiance measurements up to 5 nm.

Acknowledgments The SORCE mission is supported at LASP by the NASA contract NAS5-97045. We are grateful to the many dedicated SORCE team members at LASP, GSFC, NRL, and Orbital (now NGIS) who supported the SORCE mission over the past two decades. The pre-flight calibrations of the XPS photodiodes at NIST by Rob Vest and calibrations of under-flight rocket instruments at NIST SURF with Mitch Furst are fundamental for producing high-quality XPS science data products.

Data Availability The SORCE public data products are described on the SORCE website at lasp.colorado.edu/sorce/data/. Data files, and software to read them, are available for direct download from this web site. SORCE data products are delivered and archived at the Goddard Earth Science (GES) Data and Information Services Center (DISC) at disc.sci.gsfc.nasa.gov/SORCE/data-holdings. In addition, the LISIRD website at lasp.colorado.edu/lisird/ provides interactive access to the SORCE solar irradiance data, where they coexist with related solar irradiance data products from other missions.

Declarations

Disclosure of Potential Conflicts of Interest The authors declare no conflicts of interest.

Open Access This article is licensed under a Creative Commons Attribution 4.0 International License, which permits use, sharing, adaptation, distribution and reproduction in any medium or format, as long as you give appropriate credit to the original author(s) and the source, provide a link to the Creative Commons licence, and indicate if changes were made. The images or other third party material in this article are included in the article's Creative Commons licence, unless indicated otherwise in a credit line to the material. If material is not included in the article's Creative Commons licence and your intended use is not permitted by statutory regulation or exceeds the permitted use, you will need to obtain permission directly from the copyright holder. To view a copy of this licence, visit <http://creativecommons.org/licenses/by/4.0/>.

References

- Arp, U., Friedman, R., Furst, M.L., Makar, S., Shaw, P.-S.: 2000, SURF III – an improved storage ring for radiometry. *Metrologia* **37**, 357. DOI. ADS.
- BenMoussa, A., Gissot, S., Schühle, U., Del Zanna, G., Auchère, F., Mekaoui, S., Jones, A.R., Walton, D., Eyles, C.J., Thuillier, G., Seaton, D., Dammach, I.E., Cessateur, G., Meftah, M., Andretta, V., Berghmans, D., Bewsher, D., Bolsée, D., Bradley, L., Brown, D.S., Chamberlin, P.C., Dewitte, S., Didkovsky, L.V., Dominique, M., Eparvier, F.G., Foujols, T., Gillotay, D., Giordanengo, B., Halain, J.P., Hock, R.A., Irbah, A., Jeppesen, C., Judge, D.L., Kretzschmar, M., McMullin, D.R., Nicula, B., Schmutz, W., Ucker, G., Wieman, S., Woodraska, D., Woods, T.N.: 2013, On-orbit degradation of solar instruments. *Solar Phys.* **288**, 389. DOI. ADS.
- Chamberlin, P.C., Eparvier, F.G., Knoer, V., Leise, H., Pankratz, A., Snow, M., Templeman, B., Thiemann, E.M.B., Woodraska, D.L., Woods, T.N.: 2020, The Flare Irradiance Spectral Model-Version 2 (FISM2). *Space Weather* **18**, e2020SW002588. DOI. ADS.
- Del Zanna, G., Dere, K.P., Young, P.R., Landi, E., Mason, H.E.: 2015, CHIANTI – an atomic database for emission lines. Version 8. *Astron. Astrophys.* **582**, A56. DOI. ADS.
- Dere, K.P., Landi, E., Mason, H.E., Monsignori Fossi, B.C., Young, P.R.: 1997, CHIANTI – an atomic database for emission lines. *Astron. Astrophys. Suppl.* **125**, 149. DOI. ADS.
- Didkovsky, L., Judge, D., Wieman, S., Woods, T., Jones, A.: 2012, EUV SpectroPhotometer (ESP) in extreme ultraviolet variability experiment (EVE): algorithms and calibrations. *Solar Phys.* **275**, 179. DOI. ADS.
- Ermolli, I., Matthes, K., Dudok de Wit, T., Krivova, N.A., Tourpali, K., Weber, M., Unruh, Y.C., Gray, L., Langematz, U., Pilewskie, P., Rozanov, E., Schmutz, W., Shapiro, A., Solanki, S.K., Woods, T.N.: 2013, Recent variability of the solar spectral irradiance and its impact on climate modelling. *Atmos. Chem. Phys.* **13**, 3945. DOI. ADS.
- Garcia, H.A.: 2000, Thermal-spatial analysis of medium and large solar flares, 1976, to 1996. *Astrophys. J. Suppl. Ser.* **127**, 189. DOI. ADS.
- Hochedez, J.-F., Schmutz, W., Stockman, Y., Schühle, U., Benmoussa, A., Koller, S., Haenen, K., Berghmans, D., Defise, J.-M., Halain, J.-P., Theissen, A., Delouille, V., Slemzin, V., Gillotay, D., Fussen, D., Dominique, M., Vanhellemont, F., McMullin, D., Kretzschmar, M., Mitrofanov, A., Nicula, B., Wauters, L., Roth, H., Rozanov, E., Rüedi, I., Wehrli, C., Soltani, A., Amano, H., van der Linden, R., Zhukov, A., Clette, F., Koizumi, S., Mortet, V., Remes, Z., Petersen, R., Nesládek, M., D'Olieslaeger, M., Roggen, J., Rochus, P.: 2006, LYRA, a solar UV radiometer on Proba2. *Adv. Space Res.* **37**, 303. DOI. ADS.
- Hock, R.A., Woodraska, D., Woods, T.N.: 2013, Using SDO EVE data as a proxy for GOES XRS B 1-8 angstrom. *Space Weather* **11**, 262. DOI. ADS.
- Hock, R.A., Chamberlin, P.C., Woods, T.N., Crotser, D., Eparvier, F.G., Woodraska, D.L., Woods, E.C.: 2012, Extreme ultraviolet variability experiment (EVE) multiple EUV grating spectrographs (MEGS): radiometric calibrations and results. *Solar Phys.* **275**, 145. DOI. ADS.
- Judge, D.L., McMullin, D.R., Ogawa, H.S., Hovestadt, D., Klecker, B., Hilchenbach, M., Mobius, E., Canfield, L.R., Vest, R.E., Watts, R., Tarrío, C., Kuehne, M., Wurz, P.: 1998, First solar EUV irradiances obtained from SOHO by the CELIAS/SEM. *Solar Phys.* **177**, 161. DOI. ADS.
- Landi, E., Young, P.R., Dere, K.P., Del Zanna, G., Mason, H.E.: 2013, CHIANTI—an atomic database for emission lines. XIII. Soft X-ray improvements and other changes. *Astrophys. J.* **763**, 86. DOI. ADS.
- Lean, J., Rottman, G., Harder, J., Kopp, G.: 2005, SORCE contributions to new understanding of global change and solar variability. *Solar Phys.* **230**, 27. DOI. ADS.
- Mason, J.P., Woods, T.N., Caspi, A., Chamberlin, P.C., Moore, C., Jones, A., Kohnert, R., Li, X., Palo, S., Solomon, S.C.: 2016, Miniature X-ray solar spectrometer: a science-oriented, university 3U CubeSat. *J. Spacecr. Rockets* **53**, 328. DOI. ADS.
- Mason, J.P., Woods, T.N., Chamberlin, P.C., Jones, A., Kohnert, R., Schwab, B., Sewell, R., Caspi, A., Moore, C.S., Palo, S., Solomon, S.C., Warren, H.: 2020, MinXSS-2 CubeSat mission overview: improvements from the successful MinXSS-1 mission. *Adv. Space Res.* **66**, 3328. DOI. ADS.
- McClintock, W.E., Rottman, G.J., Woods, T.N.: 2005, Solar-stellar irradiance comparison experiment II (solstice II): instrument concept and design. *Solar Phys.* **230**, 225. DOI. ADS.
- McClintock, W.E., Snow, M., Woods, T.N.: 2005, Solar-stellar irradiance comparison experiment II (SOLSTICE II): pre-launch and on-orbit calibrations. *Solar Phys.* **230**, 259. DOI. ADS.
- Mithun, N.P.S., Vadawale, S.V., Sarkar, A., Shanmugam, M., Patel, A.R., Mondal, B., Joshi, B., Janardhan, P., Adalja, H.L., Goyal, S.K., Ladiya, T., Tiwari, N.K., Singh, N., Kumar, S., Tiwari, M.K., Modi, M.H., Bhardwaj, A.: 2020, Solar X-ray monitor on board the chandrayaan-2 orbiter: in-flight performance and science prospects. *Solar Phys.* **295**, 139. DOI. ADS.
- Moore, C.S., Caspi, A., Woods, T.N., Chamberlin, P.C., Dennis, B.R., Jones, A.R., Mason, J.P., Schwartz, R.A., Tolbert, A.K.: 2018, The instruments and capabilities of the miniature X-ray solar spectrometer (MinXSS) CubeSats. *Solar Phys.* **293**, 21. DOI. ADS.

- Pilewskie, P., Rottman, G., Richard, E.: 2005, An overview of the disposition of solar radiation in the lower atmosphere: connections to the SORCE mission and climate change. *Solar Phys.* **230**, 55. DOI. ADS.
- Raulin, J.-P., Trottet, G., Kretschmar, M., Macotela, E.L., Racini, A., Bertoi, F.C.P., Dammasch, I.E.: 2013, Response of the low ionosphere to X-ray and Lyman- α solar flare emissions. *J. Geophys. Res.* **118**, 570. DOI. ADS.
- Richard, E., Harber, D., Drake, G., Rutkowski, J., Castleman, Z., Smith, M., Sprunck, J., Zheng, W., Smith, P., Fisher, M., Sims, A., Cervelli, B., Fowle, M., Miller, M., Chambliss, M., Woods, T., Pilewskie, P., Yung, C., Stephens, M., Tomlin, N., White, M., Lehman, J.: 2019, Compact spectral irradiance monitor flight demonstration mission. In: Pagano, T.S., Norton, C.D., Babu, S.R. (eds.) *CubeSats and SmallSats for Remote Sensing III, Proc. Soc. Photo-Opt. Instrum. Eng. (SPIE) CS-11131*, 15. DOI. ADS.
- Schmidtke, G., Brunner, R., Eberhard, D., Halford, B., Klocke, U., Knothe, M., Konz, W., Schmidtke, G., Brunner, R., Eberhard, D., Halford, B., Klocke, U., Knothe, M., Konz, W., Riedel, W.-J., Wolf, H.: 2006, SOL ACES: auto-calibrating EUV/UV spectrometers for measurements onboard the international space station. *Adv. Space Res.* **37**, 273. DOI. ADS.
- Schwab, B.D., Sewell, R.H.A., Woods, T.N., Caspi, A., Mason, J.P., Moore, C.: 2020, Soft X-ray observations of quiescent solar active regions using the novel dual-zone aperture X-ray solar spectrometer. *Astrophys. J.* **904**, 20. DOI. ADS.
- Snow, M., McClintock, W., Woods, T.N., Elliott, J.: 2022, SOLSTICE instrument updated science processing algorithms. *Solar Phys.* **297**, 55. DOI. ADS.
- Sylwester, J., Kowalinski, M., Gburek, S., Siarkowski, M., Kuzin, S., Farnik, F., Reale, F., Phillips, K.J.H., BakaNa, J., Gryciuk, M., Podgorski, P., Sylwester, B.: 2012, SphinX measurements of the 2009 solar minimum X-ray emission. *Astrophys. J.* **751**, 111. DOI. ADS.
- Warren, H.P., Mariska, J.T., Doschek, G.A.: 2013, Observations of thermal flare plasma with the EUV variability experiment. *Astrophys. J.* **770**, 116. DOI. ADS.
- Woods, T.N., Rottman, G.: 2005, XUV photometer system (XPS): solar variations during the SORCE mission. *Solar Phys.* **230**, 375. DOI. ADS.
- Woods, T.N., Rottman, G., Vest, R.: 2005, XUV photometer system (XPS): overview and calibrations. *Solar Phys.* **230**, 345. DOI. ADS.
- Woods, T., Rottman, G., Russell, C., Knapp, B.: 1998, In-flight degradation results for the UARS SOLSTICE. *Instrument. Metrol.* **35**, 619. DOI. ADS.
- Woods, T.N., Eparvier, F.G., Bailey, S.M., Chamberlin, P.C., Lean, J., Rottman, G.J., Solomon, S.C., Tobiska, W.K., Woodraska, D.L.: 2005, Solar EUV experiment (SEE): mission overview and first results. *J. Geophys. Res. Space Phys.* **110**, A01312. DOI. ADS.
- Woods, T.N., Chamberlin, P.C., Peterson, W.K., Meier, R.R., Richards, P.G., Strickland, D.J., Lu, G., Qian, L., Solomon, S.C., Iijima, B.A., Mannucci, A.J., Tsurutani, B.T.: 2008, XUV photometer system (XPS): improved solar irradiance algorithm using CHIANTI spectral models. *Solar Phys.* **250**, 235. DOI. ADS.
- Woods, T.N., Eparvier, F.G., Hock, R., Jones, A.R., Woodraska, D., Judge, D., Didkovsky, L., Lean, J., Mariska, J., Warren, H., McMullin, D., Chamberlin, P., Berthiaume, G., Bailey, S., Fuller-Rowell, T., Sojka, J., Tobiska, W.K., Viereck, R.: 2012, Extreme ultraviolet variability experiment (EVE) on the solar dynamics observatory (SDO): overview of science objectives, instrument design, data products, and model developments. *Solar Phys.* **275**, 115. DOI. ADS.
- Woods, T.N., Caspi, A., Chamberlin, P.C., Jones, A., Kohnert, R., Mason, J.P., Moore, C.S., Palo, S., Rouleau, C., Solomon, S.C., Machol, J., Viereck, R.: 2017, New solar irradiance measurements from the miniature X-ray solar spectrometer CubeSat. *Astrophys. J.* **835**, 122. DOI. ADS.
- Woods, T.N., Harder, J.W., Kopp, G., McCabe, D., Rottman, G., Ryan, S., Snow, M.: 2021, Overview of the solar radiation and climate experiment (SORCE) seventeen-year mission. *Solar Phys.* **296**, 127. DOI. ADS.
- Woods, T.N., Harder, J., Kopp, G., Snow, M.: 2022, Solar cycle variability results from the SORCE mission. *Solar Phys.* **297**, 43. DOI. ADS.